analytical chemistry

pubs.acs.org/ac Article

In Situ Controllable Generation of Copper Nanoclusters Confined in a Poly-L-Cysteine Porous Film with Enhanced Electrochemiluminescence for Alkaline Phosphatase Detection

Mei-Chen Pan, Yan-Mei Lei, Ya-Qin Chai, Ruo Yuan, and Ying Zhuo*

Cite This: *Anal. Chem.* 2020, 92, 13581−13587 Read Online

ACCESS | Metrics & More | Article Recommendations | Supporting Information

ABSTRACT: Copper nanoclusters (Cu NCs) as emerging luminescent metal NCs are gaining increasing attention owing to the comparatively low cost and high abundance of the Cu element in nature. However, it remains challenging to manipulate the optical properties of Cu NCs. Unlike most dispersed Cu NCs, whose luminescence efficiency was restricted by nonexcited relaxation, the Cu NCs confined in a porous poly-L-cysteine (poly-L-Cys) film were generated controllably with enhanced electrochemiluminescence (ECL) by in situ electrochemical reduction. Specifically, poly-L-Cys provided a porous structure to regulate the generation of Cu NCs within its holes, which not only increased the restriction on the intramolecular vibration and rotation of the ligands but also expedited the electron transfer near the electrode surface, reflecting in an enhancement of the ECL signal and efficiency. As an application of the confined Cu NCs, an ECL biosensor with high performance was constructed skillfully for highly sensitive detection of alkaline phosphatase (ALP), which adopted Cu NCs as the ECL luminophore and poly-L-Cys as a coreaction accelerator in a novel ECL ternary system (Cu NCs/$S_2O_8^{2-}$/poly-L-Cys). Furthermore, an ingenious target amplification based on the combination of a DNA walker and click chemistry was developed to convert ALP to DNA strands efficiently, achieving great improvement in the recognition efficiency. As a result, the biosensor had a low detection limit (9.5×10^{-7} U·L^{-1}) and a wide linear range (10^{-8}−10^{-2} U·L^{-1}) for ALP detection, which showed great promise for the detection of non-nucleic acid targets and the diagnosis of diseases.

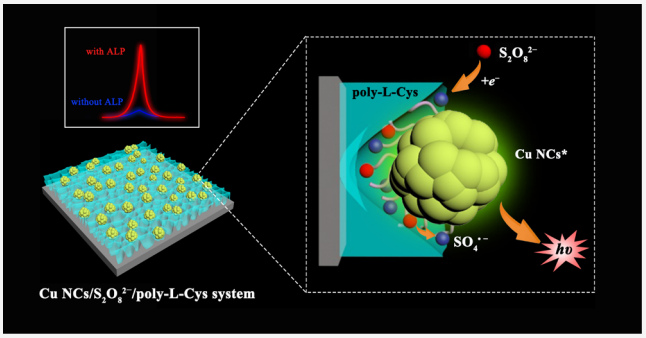

INTRODUCTION

Metal nanoclusters (NCs), used as an emerging kind of electrochemiluminescence (ECL) luminophores,[1] have received substantial attention in biolabeling, bioimaging, and biosensing by virtue of their excellent biocompatibility,[2−5] low environmental risk, and stability against photobleaching,[6] which are distinct from traditional organic luminophores.[7] Although outstanding progress has been made in noble metal NCs (mainly gold and silver),[8−10] copper nanoclusters (Cu NCs) have been extensively investigated likewise[11] due to the comparatively low cost and high abundance of the Cu element in nature.[12] However, the synthesis of Cu NCs with high stability is fundamentally limited by the easy aggregation due to high surface energy and oxidizability when exposed to air.[4,13] Considerable efforts have been directed toward exploring suitable capping ligands to enhance stability.[14,15] For example, Wei and co-workers utilized 2-mercapto-5-*n*-propylpyrimidine as a protecting ligand to prepare Cu NCs with a wet chemical reduction strategy in an organic solution.[16] Despite distinct luminescence of the dispersed Cu NCs, the ECL efficiency was restricted by the low local concentration and electron-transfer efficiency, where nonexcited relaxation suppresses the emission.[17] In this perspective, the quest for a favorable reaction microenvironment, which could concentrate the Cu NCs and speed up the electron-transfer reaction,[18] is imperative to increase the stability and the ECL efficiency of Cu NCs.

Porous materials, whose channels and voids allow the integration of various units into robust porous networks, have emerged as promising candidates for providing a confined reaction microenvironment. It was reported that the confined space could not only accommodate the electrochemically active substances within holes but also facilitate electron and mass transfer in electrochemical reactions.[19] Inspired by the abilities of porosity in electrochemistry, it was inferred that porosity was conducive to the shortening of spatial diffusion distance and the survival of radicals, both of which contributed

Received: August 4, 2020
Accepted: September 7, 2020
Published: September 7, 2020

https://dx.doi.org/10.1021/acs.analchem.0c03312
Anal. Chem. 2020, 92, 13581−13587

Scheme 1. Schematic Illustration of the Proposed ECL Biosensor for ALP Detection: Preparation Steps of In Situ Controllable Generation of Cu NCs Confined in a Poly-L-Cys Porous Film (A) and Target-Initiated Amplification Based on Click Chemistry and a DNA Walker (B)

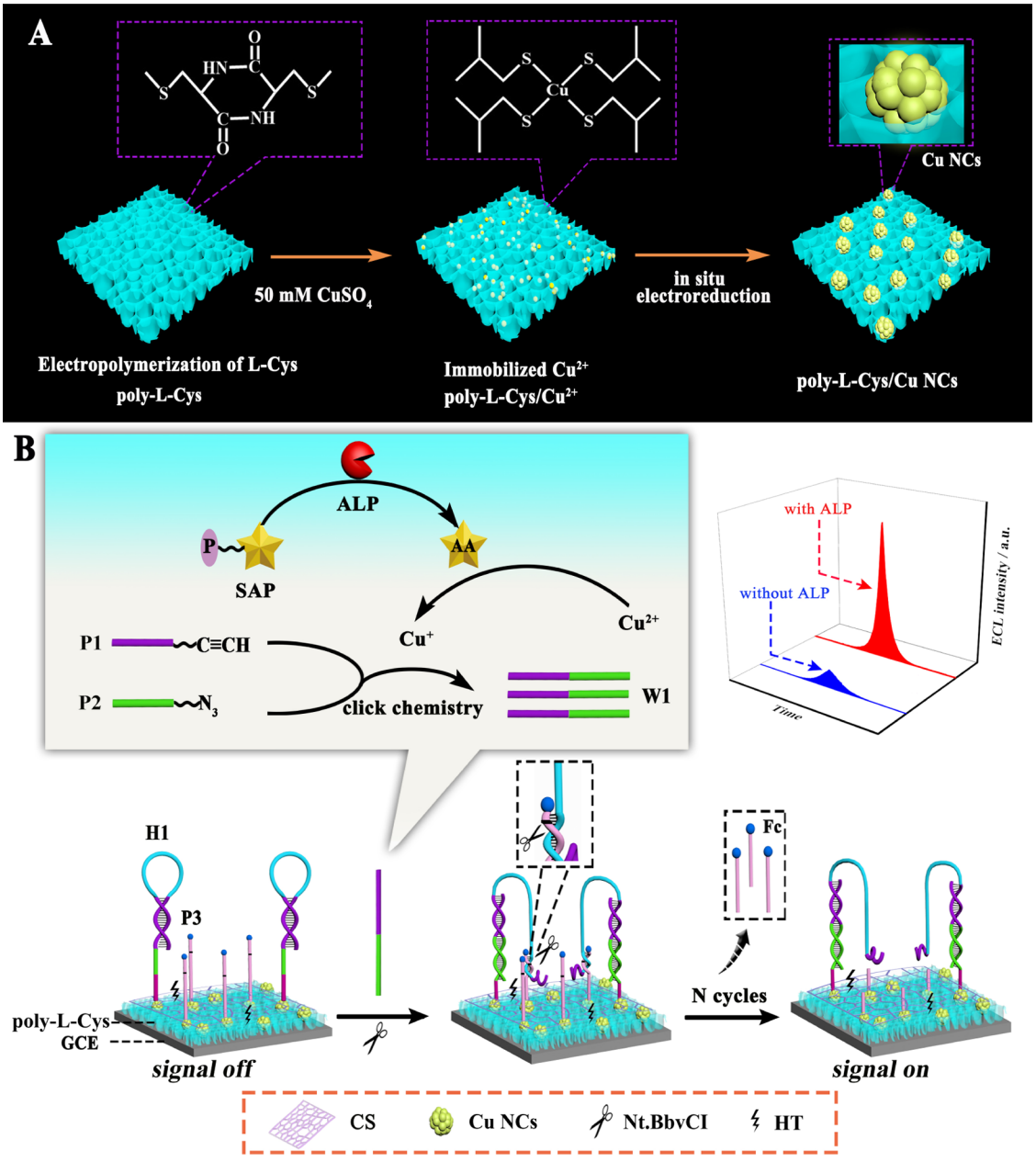

to the subsequent recombination of electrons and holes for ECL emission. Recently, our group first prepared stannic oxide (SnO_2) nanocrystal xerogel with a porous structure, which enhanced the ECL by tenfold compared with that of discrete SnO_2 NCs.[20] Zeng and colleagues selected covalent organic frameworks with a porous structure as microreactors to assemble tris(2,2′-bipyridyl) ruthenium(II) ($Ru(bpy)_3^{2+}$), which realized the confinement-enhanced ECL.[21] However, the construction of these solid-state ECL biosensors involved an additional modification procedure on the electrode surface for immobilizing porous materials, resulting in time consumption and limited reproducibility.[22] With the intrinsic properties in a straightforward procedure and highly controllable implementation, the electrodeposition technique gave a fresh impetus to control the synthesis and stowage of materials simultaneously.[23] Herein, poly-L-cysteine (poly-L-Cys) was deposited by electropolymerization as a template, where Cu NCs could be generated controllably by means of in situ electrochemical reduction using electrostatic deposition (Scheme 1A). Intriguingly, the porous poly-L-Cys structure could provide abundant accessible surface sites for concentrating Cu NCs within the holes, which not only improved stability to Cu NCs but also expedited the electron transfer near the electrode surface.

Alkaline phosphatase (ALP) as a kind of hydrolytic enzyme plays an important role in the cell signaling pathways, the activity of which belongs to a routine index of blood examination.[24] To date, many photo/electroanalytical methods have been developed to determine ALP, whose sensitivities were limited because of the lack of target amplification. The

https://dx.doi.org/10.1021/acs.analchem.0c03312
Anal. Chem. 2020, 92, 13581−13587

nucleic acid signal amplification technique has been widely applied in biological detection,[25] which transforms the trace targets into enormous nucleic acid molecular output for signal amplification.[26] Noticeably, a DNA walker, as one of the signal amplification strategies by walking along certain tracks to output DNA autonomously, plays a well-established role in the increment of local concentration and recognition efficiency.[27] Thus, an ECL biosensor with excellent performance was constructed for ALP detection (as shown in Scheme 1), which adopted Cu NCs confined in the poly-L-Cys film as an ECL luminophore, with poly-L-Cys as a coreaction accelerator in a novel ECL ternary system (Cu NCs/$S_2O_8^{2-}$/poly-L-Cys). In addition, the DNA walker-based target amplification strategy was developed to convert ALP to DNA strands efficiently with the aid of click chemistry, which made it a powerful tool to achieve great improvement of sensitivity and recognition efficiency. As illustrated in Scheme 1B, a highly specific enzyme catalysis reaction and high-yield click chemistry were combined to transfer ALP into abundant DNA strands to activate the DNA walker. Simultaneously, a very low ECL signal was obtained from the electrode modified by hairpin probe H1 and quenching probe P3 (a ferrocene-modified DNA strand, Fc-DNA) ("off" state).[28] Once the target ALP appeared, sodium L-ascorbyl-2-phosphate (SAP) was dephosphorylated to form ascorbic acid (AA) as a reducing agent, triggering a click chemical reaction that links a single chain containing alkynyl (alkynyl-DNA, P1) to a single chain containing azido (alkynyl-DNA, P2) to form a longer single chain W1. Next, W1 opened hairpin H1 on the surface of the electrode to reveal the protruding single strand fragment (as a DNA walker), which could hybridize with the nearby quenching probe P3. Remarkably, under the splicing action of Nt.BbvCI, Fc was released and the ECL signal was recovered ("on" state). Consequently, the ECL intensity increased dramatically as the concentration of ALP increased to realize the sensitive detection of ALP.

EXPERIMENTAL SECTION

Preparation of ECL Biosensors Based on In Situ Controllable Generation of Cu NCs. Prior to the modification, the glassy carbon electrode (GCE) was well dispersed by sonication and scouring to obtain a clean surface (as shown in the Supporting Information). Then, the clean GCE was dipped in L-Cys aqueous solution (2 mL, 0.02 M, pH 1.0) with cyclic voltammetry (CV) electrodeposition at the potential from −0.5 to 1.0 V at 100 mV s^{-1} rate for 15 cycles to obtain a porous poly-L-Cys film modified electrode (poly-L-Cys/GCE). Next, the resultant electrode was incubated with 50 mM $CuSO_4$ solution (10 μL) for 10 min at room temperature to incorporate Cu^{2+} via Cu−S bonds. After rinsing with deionized water to eliminate the uncombined Cu^{2+}, the resultant electrode was immersed in phosphate buffer saline (PBS, 0.1 M, pH 7.4) for in situ electrochemical reduction of Cu^{2+} with electrostatic deposition (the applied potential was −1.0 V for 10 s) to generate the Cu NCs in the poly-L-Cys porous film (Cu NCs/poly-L-Cys/GCE). The following procedure was the dropwise addition of chitosan (CS, 5 μL, 0.02%) solution onto the modified GCE, which was dried at room temperature. Next, 15 μL of mixed solution, composed of 5 μL of H1 (0.5 μM), 5 μL of P3 (5 μM), and 5 μL of 4-(*N*-maleimidomethyl) cyclohexane-1-carboxylic acid 3-sulfo-*N*-hydroxysuccinimide ester sodium salt (Sulfo-SMCC, 20 μM), was dropped onto the resultant GCE and incubated for 1.5 h. Then, 15 μL of hexanethiol solution (HT, 1 mM) was cast on the modified GCE for 40 min to choke the nonspecific adsorption sites. Finally, the prepared biosensor was stored at 4 °C for further use.

Target-Initiated Amplification Based on Click Chemistry. ALP was converted into DNA strands based on click chemistry by the following steps. Primarily, the ALP solution with different concentrations was added in 15 mL of mixed solution containing 3 mL of P1 (alkynyl-DNA, 5 μM), P2 (azido-DNA, 5 μM), SAP (5 μM), and $CuSO_4$ (0.1 mM) and incubated at 37 °C for 1.5 h. SAP was catalyzed by ALP to generate AA, resulting in the reduction of Cu^{2+} to Cu^{+}. Synchronously, the click chemical reaction was triggered by Cu^{+} to produce massive single strands W1 (the linkage of P1 and P2), which were used to initiate the subsequent amplification reaction.

Subsequently, 15 μL of resultant solution (containing W1) was mixed with 3 μL of Nt.BbvCI (100 U mL^{-1}), which was cast on the modified electrode and incubated for 1.5 h. W1 as the initiator could hybridize with H1 to expose a single-stranded terminal, which as activated DNA walker hybridized with the nearby quenching probe P3 to make Fc release under the shearing action of Nt.BbvCI. Sequentially, the released walker further hybridized with another nearby P3, realizing autonomous DNA walking on the track to release Fc. Completing each step, the modified electrode was rinsed with PBS (0.1 M, pH 7.4) to remove nonspecifically bonded conjugates.

ECL Measurement Procedure. Considering that the ECL intensity increased dramatically when the concentration of ALP increased, the biosensor could be used to realize the sensitive detection of ALP. The ECL responses were detected by an MPI-E multifunctional electrochemical and chemiluminescent analytical system in 2 mL of PBS (0.1 M, pH 7.4) containing 10 mM $S_2O_8^{2-}$ by cycling the potential from −2 to 0 V at a scanning rate of 300 mV s^{-1} and setting the voltage of the photomultiplier tube (PMT) to 800 V.

RESULTS AND DISCUSSION

Characterization of the Poly-L-Cys Film and the In Situ Controllable Generation of Cu NCs. The morphology and size of poly-L-Cys were characterized by scanning electron microscopy (SEM), as shown in Figure 1A. It was clearly revealed that poly-L-Cys had a porous film structure, distributing abundant pores with diameters of ∼100 nm on its surface. Compared with the SEM image of the poly-L-Cys film, Figure 1B clearly displays that some nanocube structures were located in the pores of the poly-L-Cys film, which was corresponding to the confined Cu NCs. Energy dispersive X-ray spectroscopy (EDS) proved the presence of the Cu element (Figure 1C), which further visually illustrated the generation of Cu NCs. As distinctly shown in the high-resolution transmission electron microscopy (HRTEM) images of Cu NCs (Figure 1D), the interplanar spacing of lattice fringes was 0.207 nm (the inset of Figure 1D), corresponding to the (111) planes of face-centered Cu (JCPDS 89-2838), which confirmed the presence of Cu atoms and the crystal structure of Cu NCs.[13]

X-ray photoelectron spectroscopy (XPS) was used to analyze the oxidation state of the copper element in the Cu NCs/poly-L-Cys compound. Figure 1E showed the XPS survey spectrum, which exhibited peaks corresponding to all of the elements C, O, N, S, and Cu. The XPS survey spectrum of the

https://dx.doi.org/10.1021/acs.analchem.0c03312
Anal. Chem. 2020, 92, 13581−13587

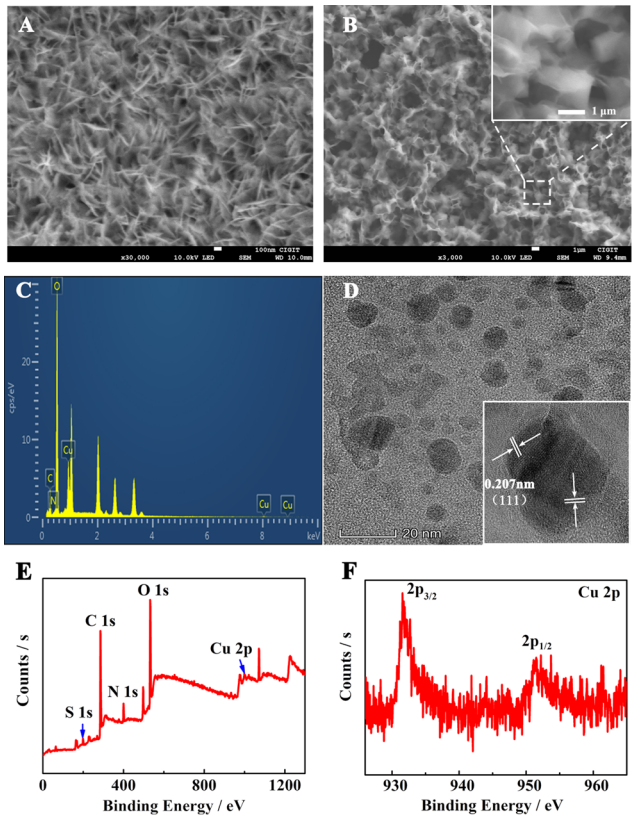

Figure 1. SEM characterization of the porous poly-L-Cys film with a scale bar of 100 nm (A), in situ controllable generation of Cu NCs confined in the poly-L-Cys film with a scale bar of 1 μm and the inset corresponding to the enlarged image (B). EDS spectrum of the Cu NCs (C). HRTEM characterization of the Cu NCs and the inset corresponding to the crystalline structure of Cu NCs (D). XPS spectra showing the full region of the Cu NCs (E) and Cu 2p region (F).

Cu 2p region exhibited two intense peaks at 953.6 and 932.7 eV (Figure 1F), which corresponded to Cu 2p1/2 and 2p3/2, belonging to Cu (0). Moreover, there was no characteristic peak at around 942 eV, which implied the absence of Cu^{2+} in the Cu NCs.[29]

ECL and fluorescence (FL) spectra were obtained to characterize the optical properties of Cu NCs. According to the three-dimensional (3D) ECL spectrum (Figure 2A) and heat map image (Figure 2B), the ECL maximum wavelength of Cu NCs was located at 596.2 nm at a potential of −2.0 V, obviously differing from the emission peak of $S_2O_8^{2-}$ (at around 675 nm), demonstrating that more excited states of the luminophore (Cu NCs) were produced with the aid of $SO_4^{\bullet-}$ generated by $S_2O_8^{2-}$ as a coreactant. As depicted in Figure 2C, the FL spectrum of Cu NCs showed the maximum wavelength at 463.8 nm (red curve), with the excitation peak at around 369.6 nm (blue curve). Under UV-light irradiation (λ = 365 nm), the solution of the Cu NCs was bright blue, while it was colorless under visible light (the inset of Figure 2C). Compared with the FL emission peak of the Cu NCs, the maximum ECL emission peak in Figure 2D had an obvious 132 nm red shift, probably owing to the surface-state-related ECL emission.[30]

Possible ECL Mechanism of the Cu NCs/$S_2O_8^{2-}$/Poly-L-Cys System. To explore the ECL mechanism of the Cu NCs/$S_2O_8^{2-}$/poly-L-Cys system, ECL and CV responses of different

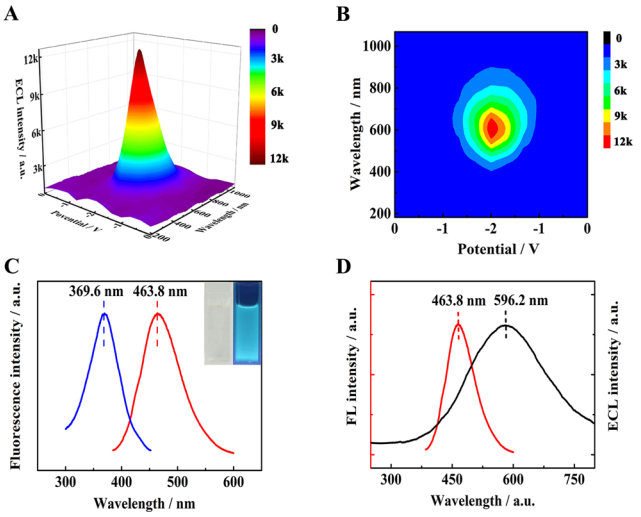

Figure 2. 3D ECL spectrum (A) and heat map image (B) of Cu NC in PBS (0.1 M, pH 7.4) containing 10 mM $S_2O_8^{2-}$. Fluorescence excitation spectra and emission spectra of Cu NCs (C). The inset of (C) showed the photographs of the solution of Cu NCs under visible-light irradiation (left) and UV-light irradiation (blue). Fluorescence spectrum and maximum ECL spectrum of the prepared Cu NCs at −2.0 V (D).

modified electrodes were measured at the scanning potential range from −2.0 to 0 V, as shown in Figure 3. First, the Cu

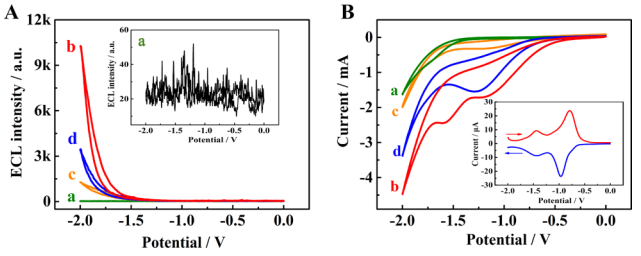

Figure 3. Synchronous ECL (A) and CV (B) curves of different electrodes: Cu NCs/poly-L-Cys/GCE in PBS (0.1 M, pH 7.4) without (curve a) and with (curve b) 10 mM $S_2O_8^{2-}$; bare GCE (curve c), and poly-L-Cys/GCE (curve d) in PBS (0.1 M, pH 7.4) containing 10 mM $S_2O_8^{2-}$ (the sweep voltage range was −2.0− 0 V). The inset of (B) showed the DPV of the Cu NCs/poly-L-Cys/GCE in tetrabutylammonium hexafluorophosphate (TBAPF6); the arrows indicated the scan direction.

NCs-modified GCE (Cu NCs/poly-L-Cys/GCE) showed a little or no ECL signal in PBS (Figure 3A, curve a). This result was attributed to the low content of the excited-state Cu NCs (Cu NCs*) produced because of the lack of a coreactant.[31] The corresponding CV curve had the weakest redox peak (Figure 3B, curve a), suggesting the low concentration of the reductive species ($Cu\ NCs^{-}$). Due to the suppression of the background current, the redox behavior of Cu NCs could not be investigated adequately. Thus, the differential pulse voltammetry (DPV) response of Cu NCs was measured in tetrabutylammonium hexafluorophosphate (TBAPF6) (the inset of Figure 3B). There were two well-resolved reversible DPV peaks, one of which located at ∼ −1.5V further verified that Cu NCs were reduced to $Cu\ NCs^{-}$. Subsequently, when Cu NCs/poly-L-Cys/GCE were detected in PBS (0.1 M, pH 7.4) containing 10 mM $S_2O_8^{2-}$, it was observed that the ECL signal significantly enhanced to as high as ∼14 400 a.u. in the

https://dx.doi.org/10.1021/acs.analchem.0c03312
Anal. Chem. 2020, 92, 13581−13587

ECL−potential curve (Figure 3A, curve b). Furthermore, note that the reduction peak current of Cu NCs increased continuously in the current−potential curve (Figure 3B, curve b). It was speculated that $S_2O_8^{2-}$ as a redox-active substance was reduced to a sulfate radical ($SO_4^{\bullet-}$), which reacted with Cu NCs$^-$ to produce more Cu NCs*. When bare GCE was detected in 0.1 M PBS (pH 7.4) containing 10 mM $S_2O_8^{2-}$, an obvious ECL signal (~1271 a.u., Figure 3A, curve c) was observed, which was attributed to the radiation of $^1(O_2)_2$*.[32] Meanwhile, the corresponding CV response had an obvious reduction peak at −1.1 V (Figure 3B, curve c) because of the electrochemical reaction of $S_2O_8^{2-}$.[7] Subsequently, when poly-L-Cys/GCE was measured in 10 mM $S_2O_8^{2-}$ (pH 7.4), it was observed that the ECL signal significantly enhanced about three times (~3677 a.u., Figure 3A, curve d), which manifested that poly-L-Cys as a kind of coreaction accelerator reacted with $S_2O_8^{2-}$, speeding up the reduction of $S_2O_8^{2-}$ to generate more strongly oxidized intermediates ($SO_4^{\bullet-}$). Correspondingly, it was clearly observed that the position of the reduction peak was shifted slightly from −1.1 to −1.2 V (Figure 3B, curve d), accompanied by a stronger current peak, further verifying the coreaction acceleration of $S_2O_8^{2-}$. All of the obtained results showed strong evidence that the observed emission of Cu NCs was indeed amplified by $S_2O_8^{2-}$, with poly-L-Cys as a coreaction accelerator. Consequently, the possible ECL mechanism was depicted as per the following equations

$$\text{Cu NCs} + e^- \rightarrow \text{Cu NCs}^-$$

$$S_2O_8^{2-} + e^- \xrightarrow{\text{poly-L-Cys}} SO_4^{\cdot-} + SO_4^{2-}$$

$$\text{Cu NCs}^- + SO_4^{\cdot-} \rightarrow SO_4^{2-} + \text{Cu NCs}^*$$

$$\text{Cu NCs}^* \rightarrow \text{Cu NCs} + h\nu$$

ECL Performance Comparison of the Cu NCs Synthesized by Different Ligands. To better estimate the ECL performance of the prepared Cu NCs in the $S_2O_8^{2-}$ solution (10 mM, pH 7.4), four kinds of ligands consisting of poly-L-Cys, glutathione (GSH), bovine serum albumin (BSA), and L-cysteine (L-Cys) were employed to synthesize Cu NCs for the comparison of the ECL intensity and efficiency. As shown in Figure 4A, the ECL intensities of the Cu NCs synthesized with GSH (curve b, 3722 a.u.) and L-Cys (curve *d*, 3104 a.u.) were limited. Simultaneously, the ECL intensity of the Cu NCs synthesized with BSA as the ligand (curve *c*, 6522 a.u.) was slightly higher, which could be ascribed to the fact that the BSA as a biomacromolecule could provide abundant binding sites for the arrangement of Cu NCs.[33,34] It is worth noting that the ECL intensity of the Cu NCs synthesized with poly-L-Cys reached up to 12 294 a.u. (Figure 4A, curve a), surpassing considerably those of other Cu NCs. Furthermore, the relative ECL efficiency of Cu NCs was calculated by the ratio of the ECL quantum efficiency of the Cu NCs synthesized by different templates in reference to that synthesized by poly-L-Cys (the detailed calculation process is shown in the Supporting Information). Apparently, the $\Phi/\Phi_{\text{poly-L-Cys}}$ values of the Cu NCs synthesized by other methods were less than 1 (Figure 4B), indicating that the ECL efficiency of the Cu NCs by poly-L-Cys was the highest. The reason for the exquisite ECL signal and enhanced ECL efficiency of Cu NCs was the porous poly-L-Cys film, whose significant impacts on the ECL performance of Cu NCs can be demonstrated as follows: (1) poly-L-Cys acted as a polymer ligand restricted in vibration and rotation, which reduced the nonexcited relaxation of ligands, resulting in the improvement of stability and ECL intensity; (2) poly-L-Cys also provided a porous structure that regulated the generation of Cu NCs within its holes, which improved the electron transfer efficiency between the active intermediates of Cu NCs (Cu NC$^-$) and the oxidized intermediates of $S_2O_8^{2-}$ ($SO_4^{\bullet-}$);[35] and (3) poly-L-Cys performed as a kind of coreaction accelerator speeding up the reduction of $S_2O_8^{2-}$,[32,36] which increased the amount of excited-state species (Cu NCs*) to enhance the ECL intensity of Cu NCs.

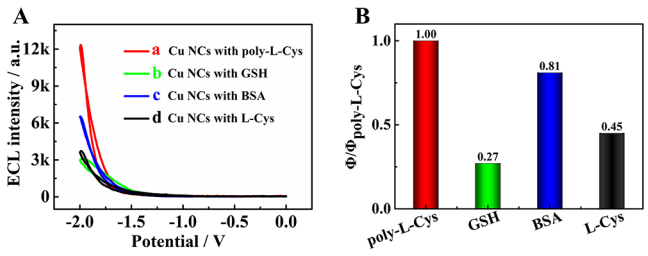

Figure 4. ECL intensity (A) and relative ECL efficiency (B) of the Cu NCs synthesized by different ligands in PBS (0.1 M, pH 7.4) containing 10 mM $S_2O_8^{2-}$.

ECL Analytical Performance of the Constructed Biosensor for ALP Detection. To identify the sensitivity of the constructed ECL biosensor, the quantitative measurement was obtained by determining ALP with different concentrations under the optimal reaction conditions. As depicted in Figure 5A, the ECL signal of the biosensor increased when the concentration of ALP increased from 10^{-8} to 10^{-2} U·L^{-1} (curves a−g). Noticeably, the ECL intensity exhibited a desirable linear relationship with the logarithm of the ALP concentration. The linear regression equation was ΔI

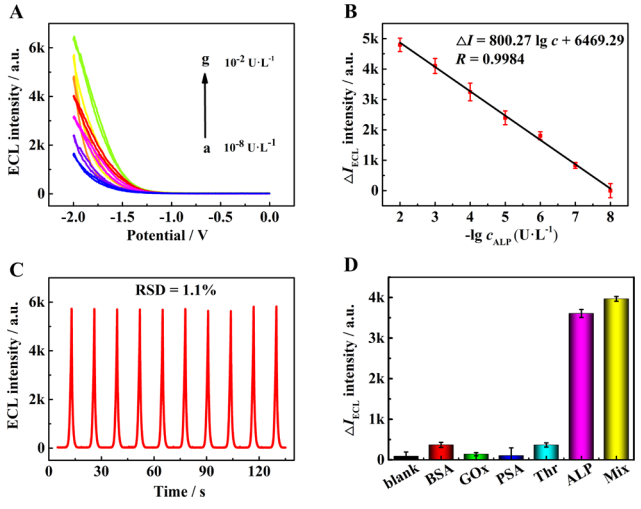

Figure 5. ECL curves of the biosensor with different concentrations of ALP in 10 mM $S_2O_8^{2-}$ (pH 7.4) (a−g): 1.0×10^{-8}, 1.0×10^{-7}, 1.0×10^{-6}, 1.0×10^{-5}, 1.0×10^{-4}, 1.0×10^{-3}, and 1.0×10^{-2} U·L^{-1}, respectively (A). Linear relationship between the change value of the ECL signal (ΔI is the difference between the ECL signal and the blank signal) and the log value of the ALP concentration (B). ECL stability of the constructed biosensor (C). Selectivity of the ECL biosensor for blank; 10^{-6} U·L^{-1} ALP; and 10^{-4} U·L^{-1} interference enzymes, including BSA, GO*x*, PSA, and Thr (D).

https://dx.doi.org/10.1021/acs.analchem.0c03312
Anal. Chem. 2020, 92, 13581−13587

= 800.27 log c + 6469.29 (Figure 5B), where ΔI is the difference between the obtained ECL intensity and the blank signal and c is the ALP concentration. Additionally, the detection limit was calculated to be 9.5×10^{-7} U·L^{-1} (S/N = 3).[37] Meanwhile, the performance comparison between this work and other biosensors for ALP detection was shown in Table S2 of the Supporting Information, which turned out that the test time of this experiment was within the acceptable range. Furthermore, it was apparent that this ECL biosensor based on in situ electrochemical controllable generation of Cu NCs owned a lower detection limit and a wider linear range.

The stability and specificity as two vital properties of biosensor were investigated. Relatively stable ECL response of continuous 10 curves could be observed for the proposed biosensor with a relative standard deviation (RSD) of 1.1% (Figure 5C), indicating the excellent stability of the biosensor. To further assess the specificity of the proposed biosensor for ALP detection, the biosensor was tested by detecting different enzymes, including bovine serum albumin (BSA), glucose oxidase (GOx), prostate-specific antigen (PSA), and thrombin (Thr). As shown in Figure 5, it was observed that the ECL responses of BSA, GOx, PSA, and Thr (10^{-4} U·L^{-1}) were ignorable and close to the blank signal compared with the presence of ALP (10^{-6} U·L^{-1}) (Figure 5D), which demonstrated the excellent selectivity of the designed biosensor for the detection of ALP.

Application of the ALP Biosensor in Human Serum. To verify the feasibility of the proposed ALP biosensor in actual sample detection, this work used the standard addition method to investigate the recovery rate of the biosensor. The ALP solution with different concentrations was added to the human serum solution (diluted 50 times by PBS) for ALP detection. The recovery concentration was calculated from the standard curve fitted before (Figure 5B). The recovery was the ratio of the detected ALP concentration to the actual concentration of ALP. The experimental results were shown in Table 1. The recoveries (95.06−106.2%) and RSDs (0.6−2.4%) were within the acceptable range, which proved that the ECL biosensor had certain application potential in the actual sample analysis.

Table 1. Actual Sample Analysis of ALP in Human Serum by the ECL Sensor

sample number	added (U·L^{-1})	found (U·L^{-1})	recovery (%)	RSD (%)
1	1.000×10^{-4}	1.062×10^{-4}	106.2	0.6
2	1.000×10^{-5}	1.005×10^{-5}	100.5	2.1
3	1.000×10^{-6}	9.506×10^{-7}	95.06	2.4

CONCLUSIONS

In summary, a highly sensitive ECL biosensor was constructed for ALP detection, with Cu NCs confined in a porous poly-L-Cys film as an ECL luminophore and poly-L-Cys as a coreaction accelerator in a novel ECL ternary system (Cu NCs/$S_2O_8^{2-}$/poly-L-Cys). The exquisite stability and enhanced ECL efficiency of the synthesized Cu NCs could be ascribed to the favorable microenvironment obtained by the porous poly-L-Cys film, which promoted the controllable formation of Cu NC aggregates confined in the pores of the poly-L-Cys film, restricted the vibration and rotation of ligands, and improved the electron-transfer efficiency between the active intermediates of Cu NCs and the oxidized intermediates of $S_2O_8^{2-}$. Moreover, the amplification of the DNA walker triggered by click chemistry provided a pathway to improve the analytical efficiency and sensitivity, which showed great application potential for the detection of multiple proteins and the diagnosis of diseases.

ASSOCIATED CONTENT

Supporting Information

The Supporting Information is available free of charge at https://pubs.acs.org/doi/10.1021/acs.analchem.0c03312.

Reagents, materials, and apparatus used in this work, ECL and CV characterizations of the biosensor establishment process, optimization of the experimental conditions, comparison of different methods for ALP detection, and relative ECL efficiencies of Cu NCs by different synthesis methods (PDF)

AUTHOR INFORMATION

Corresponding Author

Ying Zhuo − *Key Laboratory of Luminescence Analysis and Molecular Sensing (Southwest University), Ministry of Education, College of Chemistry and Chemical Engineering, Southwest University, Chongqing 400715, P. R. China;* orcid.org/0000-0002-4491-1186; Phone: +86-23-68253172; Email: yingzhuo@swu.edu.cn

Authors

Mei-Chen Pan − *Key Laboratory of Luminescence Analysis and Molecular Sensing (Southwest University), Ministry of Education, College of Chemistry and Chemical Engineering, Southwest University, Chongqing 400715, P. R. China*

Yan-Mei Lei − *Key Laboratory of Luminescence Analysis and Molecular Sensing (Southwest University), Ministry of Education, College of Chemistry and Chemical Engineering, Southwest University, Chongqing 400715, P. R. China*

Ya-Qin Chai − *Key Laboratory of Luminescence Analysis and Molecular Sensing (Southwest University), Ministry of Education, College of Chemistry and Chemical Engineering, Southwest University, Chongqing 400715, P. R. China;* orcid.org/0000-0003-4392-9592

Ruo Yuan − *Key Laboratory of Luminescence Analysis and Molecular Sensing (Southwest University), Ministry of Education, College of Chemistry and Chemical Engineering, Southwest University, Chongqing 400715, P. R. China;* orcid.org/0000-0003-3664-6236

Complete contact information is available at: https://pubs.acs.org/10.1021/acs.analchem.0c03312

Notes

The authors declare no competing financial interest.

ACKNOWLEDGMENTS

This work was financially supported by the NNSF of China (21675130, 21775124, and 21675129), the Chongqing Talents Touth Top-notch Personnel Support Program (CQYC201905067), and the Fundamental Research Funds for the Central Universities (XDJK2019TJ002), China.

REFERENCES

(1) Díez, I.; Pusa, M.; Kulmala, S.; Jiang, H.; Walther, A.; Goldmann, A. S.; Muller, A. H. E.; Ikkala, O.; Ras, R. H. A. *Angew. Chem., Int. Ed.* **2009**, *48*, 2122−2125.
(2) Daniel, M.; Astruc, D. *Chem. ReV.* **2004**, *104*, 293−346.
(3) Yang, L. N.; Wang, H. L.; Li, D. Y.; Li, L.; Lou, X. F.; Liu, H. L. *Chem. Mater.* **2018**, *30*, 5507−5515.
(4) Zhang, L. B.; Wang, E. K. *Nano Today* **2014**, *9*, 132−157.
(5) Dong, L. Y.; Li, M. L.; Zhang, S.; Li, J.; et al. *Small.* **2015**, *11*, 2571−2581.
(6) Vilar-vidal, N.; Rey, J. R.; Quintela, M. A. L. *Small* **2014**, *10*, 3632−3636.
(7) Richter, M. M. *Chem. Rev.* **2004**, *104*, 3003−3036.
(8) Zhang, Y. Y.; Feng, Q. M.; Xu, J. J.; Chen, H. Y. *ACS Appl. Mater. Interfaces* **2015**, *7*, 26307−26314.
(9) Chen, S.; Ma, H. D.; Padelford, J. W.; Qinchen, W. L.; Wang, S. X.; Zhu, M. Z.; Wang, G. L.; et al. *J. Am. Chem. Soc.* **2019**, *141*, 9603−9609.
(10) Swanick, K. N.; Hesari, M.; Workentin, M. S.; Ding, Z. F. *J. Am. Chem. Soc.* **2012**, *134*, 15205−15208.
(11) Zhao, M.; Chen, A. Y.; Huang, D.; Zhuo, Y.; Chai, Y. Q.; Yuan, R. *Anal. Chem.* **2016**, *88*, 11527−11532.
(12) Lai, W. F.; Wong, W. T.; Rogach, A. L. *Adv. Mater* **2020**, *32*, No. 1906872.
(13) Jia, X. F.; Li, J.; Wang, E. K. *Small* **2013**, *9*, 3873−3879.
(14) Wu, Z. N.; Liu, H. W.; Li, T. T.; Liu, J. L.; Yin, J.; et al. *J. Am. Chem. Soc.* **2017**, *139*, 4318−4321.
(15) Wu, Z. N.; Liu, J. L.; Gao, Y.; Liu, H. W.; Li, T. T.; et al. *J. Am. Chem. Soc.* **2015**, *137*, 12906−12913.
(16) Wei, W. T.; Lu, Y. Z.; Chen, W.; Chen, S. W. *J. Am. Chem. Soc.* **2011**, *133*, 2060−2063.
(17) Liu, P. X.; Qin, R. X.; Fu, G.; Zheng, N. F. *J. Am. Chem. Soc.* **2017**, *139*, 2122−2131.
(18) Peng, H. P.; Huang, Z. N.; Deng, H. H.; Wu, W. H.; Huang, K. Y.; Li, Z. L.; Chen, W.; Liu, J. W. *Angew. Chem., Int. Ed.* **2020**, *59*, 9982−9985.
(19) Lu, S. M.; Peng, Y. Y.; Ying, Y. L.; Long, Y. T. *Anal. Chem.* **2020**, *92*, 5621−5644.
(20) Lei, Y. M.; Zhuo, Y.; Guo, M. L.; Chai, Y. Q.; Yuan, R. *Anal. Chem.* **2020**, *92*, 2839−2846.
(21) Zeng, W. J.; Wang, K.; Liang, W. B.; Chai, Y. Q.; Yuan, R.; Zhuo, Y. *Chem. Sci.* **2020**, *11*, 5410−5414.
(22) Wei, H.; Wang, E. K. *TrAC, Trends Anal. Chem.* **2008**, *27*, 447−459.
(23) Zhou, X. J.; Harmer, A. J.; Heinig, N. F.; Leung, K. T. *Langmuir* **2004**, *20*, 5109−5113.
(24) Choi, Y. D.; Ho, N. H.; Tung, C. H. *Angew. Chem., Int. Ed.* **2007**, *46*, 707−709.
(25) Zhou, H.; Liu, J.; Xu, J. J.; Zhang, S. S.; Cheng, H. Y. *Chem. Soc. Rev.* **2018**, *47*, 1996−2019.
(26) He, L.; Lu, D. P.; Liang, H.; Xie, S. T.; Zhang, X. B.; Liu, Q. L.; Yuan, Q.; Tan, W. H. *J. Am. Chem. Soc.* **2018**, *140*, 258−263.
(27) Chen, A. Y.; Zhuo, Y.; Chai, Y. Q.; Yuan, R. *Chem Commun.* **2019**, *55*, 13932−13935.
(28) Fery-Forgues, S.; Delavaux-Nicot, B. *J. Photochem. Photobiol., A* **2000**, *132*, 137−159.
(29) Brege, J. J.; Hamilton, C. E.; Crouse, C. A.; Barron, A. R. *Nano Lett.* **2009**, *9*, 2239−2242.
(30) Zheng, L. Y.; Chi, Y. W.; Dong, Y. Q.; Lin, J. P.; Wang, B. B. *J. Am. Chem. Soc.* **2009**, *131*, 4564−4565.
(31) Zhou, Y.; Wang, H. J.; Zhuo, Y.; Chai, Y. Q.; Yuan, R. *Anal. Chem.* **2017**, *89*, 3732−3738.
(32) Reshetnyak, O. V.; Kovalchuk, E. P.; Skurski, P.; Rak, J.; Blazejowski, J. *J. Lumin.* **2003**, *105*, 27−34.
(33) Zhou, Y.; Wang, H. J.; Zhang, H.; Chai, Y. Q.; Yuan, R. *Anal. Chem.* **2018**, *90*, 3543−3549.
(34) Xie, J. P.; Zheng, Y. G.; Ying, J. Y. *J. Am. Chem. Soc.* **2009**, *131*, 888−889.
(35) Tian, R.; Zhang, S. T.; Li, M. W.; Zhou, Y. Q.; Lu, B.; Yan, D. P.; Wei, M.; Evans, D. G.; Duan, X. *Adv. Funct. Mater.* **2015**, *25*, 5006−5015.
(36) Ma, M. N.; Zhuo, Y.; Yuan, R.; Chai, Y. Q. *Anal. Chem.* **2015**, *87*, 11389−11397.
(37) Chen, T. T.; Hu, Y. H.; Cen, Y.; Chu, X.; Lu, Y. *J. Am. Chem. Soc.* **2013**, *135*, 11595−11602.

https://dx.doi.org/10.1021/acs.analchem.0c03312
Anal. Chem. 2020, 92, 13581−13587